CILAMCE 2017
Florianópolis - Santa Catarina - Brazil

FINITE ELEMENT SIMULATION OF THE DEEP-DRAWING PROCESS OF A TWO-PIECE TINPLATE CAN

Renato S. Horta
Luciano P. Moreira
renato.s.horta@gmail.com
luciano.moreira@metal.eeimvr.uff.br
Programa de Pós-graduação em Engenharia Mecânica, Universidade Federal Fluminense
Av. dos Trabalhadores 420, 27255-125, Volta Redonda, Rio de Janeiro, Brazil
Hesron W. de Oliveira
hesron.oliveira@csn.com.br
Companhia Siderúrgica Nacional
Rua 4, 33, 27265-610, Volta Redonda, Rio de Janeiro, Brazil
Programa de Pós-graduação em Engenharia Metalúrgica, Universidade Federal Fluminense
Av. dos Trabalhadores 420, 27255-125, Volta Redonda, Rio de Janeiro, Brazil
Thais M. W. Ouverney
thaismacedow@hotmail.com
Programa de Pós-graduação em Engenharia Mecânica, Universidade Federal Fluminense
Av. dos Trabalhadores 420, 27255-125, Volta Redonda, Rio de Janeiro, Brazil
Aline de S. Silva
aline_souza@id.uff.br
Graduação em Engenharia Mecânica, Universidade Federal Fluminense
Av. dos Trabalhadores 420, 27255-125, Volta Redonda, Rio de Janeiro, Brazil
Alexandre S. Francisco
afrancisco@metal.eeimvr.uff.br
Programa de Pós-graduação em Engenharia Mecânica, Universidade Federal Fluminense
Av. dos Trabalhadores 420, 27255-125, Volta Redonda, Rio de Janeiro, Brazil

Abstract. *The present study proposed a numerical investigation of the wall thinning effect during the deep drawing process of a two-piece can packaging for possible mass reduction. The investigated parameters were the friction coefficient between the tooling and the blank, the initial thickness and the plastic anisotropy of the blank. The mechanical properties of the 0.19 mm thick chromium coated SAE 1008 T3 steel sheets were determined by uniaxial tensile tests. Hooke's linear isotropic elasticity was assumed, together with the hypothesis of an isotropic hardening of the metallic sheet in the context of plastic flow theory. The anisotropic yield criterion was implemented in a subroutine in ABAQUS/Explicit. An unreplicated two-level* 2^4 *factorial design was performed. It was found that the initial blank thickness had the higher impact in the wall thinning, followed by the plastic anisotropy coefficients, with both being inversely proportional to the thinning effect. The friction coefficients showed the least influence.*

Keywords: *Finite element method, Factorial design, Sheet metal forming, Metallic packaging.*

1 INTRODUCTION

Over the years, the competition between different types of packaging materials boosted great technological advancements: thickness reduction of metallic materials, high speed production lines, closing systems that are more convenient for the consumers, among others. All those innovations demand high fidelity to the initial material specifications, namely, efficient quality control and/or performance follow up starting from the packaging design steps. In the past years, Brazil presented a consume distribution by packaging material type of 51% plastic, 27% cellulose, 17% metals and 5% glass (Campissi et al., 2011). To obtain a greater market share by offering the dairy and chemical markets a metallic packaging option more competitive compared to plastic, the steel mill Companhia Siderúrgica Nacional (CSN) started the project of a new two-piece metallic packaging produced from chromium coated SAE 1008 T3 steel sheets with 0.19 mm thickness by means of deep-drawing processes. The deep-drawing technology used to manufacture this packaging is composed of a single forming stage (package drawing). This production process eliminates the need of the body calendering and welding, in addition to the bottom deep-drawing, assembly and seaming, therefore reducing the packaging final cost and increasing the productivity. It also makes the packaging lighter, enables the use of thinner steel sheets and gives better presentation in terms of shape design.

In order to achieve thinner packaging walls for lighter packaging, it is important to better understand the wall thinning effect. Moreira et al. (2000) pointed the beneficial effect of large values of the plastic anisotropy coefficient R for reaching larger cup drawing ratios. Larger R-values lead to smaller values of the ratio between yield stresses in the drawing range and in the biaxial stretching range, thus making easier the plastic flow between the die and the blank-holder. In addition, for larger R-values there is a smaller thickening of the flange region and, thus, contributing to an easier drawing-in. Colgan and Monaghan (2003) observed in 400 tests carried out on blanks cut from drawing quality mild steel EN10130 FeP01 of 1 mm thickness that the punch/die radii have the greatest effect on the thickness of the deformed cups compared to the blank-holder force or friction effects. Marumo et al. (2007) studied the effect of initial sheet thickness in the cup-drawing process showing that the blank-holder force is strongly influenced by the blank thickness and the friction coefficient. In addition, as the initial sheet thickness decreases, the blank holding force required for preventing the wrinkling rapidly increases. Zein et al. (2014) developed a finite element model to predict the thinning and spring-back in the deep-drawing process indicating that an increase of the friction coefficient between the punch/blank increased the thinning effect of the stamped part. Also, thicker blanks had greater thinning and greater thickness variations throughout the cup.

With the purpose of preserving the designed packaging geometry, a study of material and process parameter is proposed in the present study. To investigate different plastic anisotropy scenarios of body cubic centered symmetry materials, two factors were suggested for the factorial analysis: the ratio between the R-values measured in parallel and diagonal orientations with respect to sheet rolling direction (R_0/R_{45}) and the ratio between the R-values in the transverse and diagonal orientations with respect to the rolling direction (R_{90}/R_{45}). For the sake of deep-drawing process investigation, the lubrication was also suggested for the factorial analysis. More specifically, the effect of different ratios between the Coulomb friction coefficients corresponding to the blank/punch contact and the blank/blank-holders contact (μ_P/μ_{BH}). Finally, the influence of thinner blanks on the thinning effect during deep drawing was also investigated to better understand the risks of necking. Having these four main factors in mind, a two-level 2^4 factorial design with a single replicate and a center point was performed to investigate the influence upon the thinning of the wall can packaging which usually precede the localized necking which, in turn, may result in poor product quality or else in stamped product scraps.

2 MATERIAL CHARACTERIZATION

The investigated material is a chromium coated SAE 1008 T3 steel sheet with 0.19 mm nominal thickness supplied by the Companhia Siderúrgica Nacional (CSN), Brazil.

2.1 Uniaxial tensile test

For the purpose of evaluating the mechanical properties of the chromium coated sheet, uniaxial tensile test was conducted at CSN Research Center. The tensile test machine used was an INSTRON 5585H floor model system with a load capacity of 250 kN. The equipment uses an Advanced Video Extensometer (AVE), a non-contact measuring technology that reads user marked points on the specimen surface, and the software to provide real time data such as applied load, elongation and to calculate the main test results. The dimensions of the specimen used in the uniaxial tensile test are shown in Fig. 1 (a), while the points marked in a tested specimen for the use of the AVE are shown in Fig 1 (b).

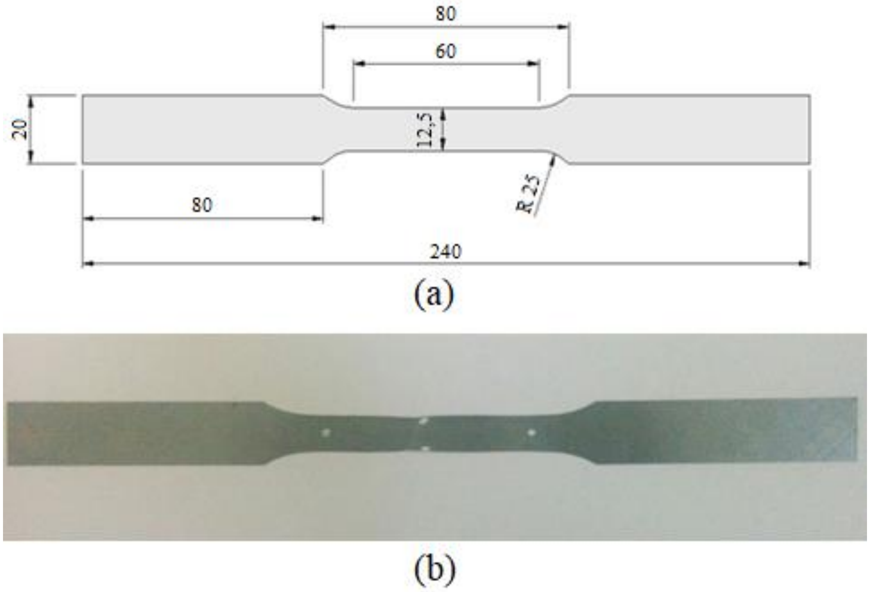

Figure 1: Uniaxial tensile specimen: (a) dimensions in mm and (b) tested specimen.

The uniaxial tensile specimens were machined by NC milling. To evaluate the initial plastic anisotropy, a total of nine specimens were tested: 3 along the rolling direction (longitudinal), 3 at 45° with respect to the rolling direction (diagonal) and 3 perpendicular to the rolling direction (transverse). The uniaxial tests were performed with a constant cross-head speed of 1 mm/min. The software provided data for elongation and load plotting, yield load, maximum load and plastic anisotropy coefficient. The stress and strain engineering data were converted to true stress-strain measures. The average plastic anisotropy coefficients for

Proceedings of the XXXVIII Iberian Latin-American Congress on Computational Methods in Engineering
P.O. Faria, R.H. Lopez, L.F.F. Miguel, W.J.S. Gomes, M. Noronha (Editores), ABMEC, Florianópolis, SC, Brazil, November 5-8, 2017.

each angular orientation were obtained and labelled as R_0, R_{45} and R_{90}. Then, planar anisotropy ΔR and normal anisotropy $\bar{R}$ coefficients were determined as:

$$\Delta R = \frac{R_0 - 2R_{45} + R_{90}}{2} \tag{1}$$

$$\bar{R} = \frac{R_0 + 2R_{45} + R_{90}}{4} \tag{2}$$

2.2 Work-hardening behavior

To describe the sheet work-hardening behavior observed in the uniaxial tensile testing, two hardening equations were adopted to relate the true-strain and true-plastic strain values. The first one is the Swift hardening equation:

$$\sigma = K(\varepsilon_0 + \varepsilon^p)^N \tag{3}$$

in which N is the strain-hardening exponent, K is the strength coefficient (MPa), ε^p is the plastic strain and ε_0 is the pre-strain term that indicates the level of stain hardening the material acquired from previous deformation process. The second hardening is the Ludwik equation:

$$\sigma = \sigma_0 + (K\varepsilon^p)^N \tag{4}$$

where σ_0 is the yield stress. The parameters of both work-hardening equations were determined from the experimental data of the uniaxial tensile tests, namely, true-stress and true-plastic strain results, by means of a nonlinear curve fitting procedure available in the commercial software Origin.

2.3 Anisotropic yield criteria

Hill's 48 anisotropic yield function is one of the most popular plasticity model to describe the behavior of orthotropic materials such as rolled sheets. In plane-stress state, which is usually assumed for thin sheet metal forming finite element modeling simulations, the yield function of Hill's 48 criterion can be cast as:

$$2F(\sigma_{ij}) = (G + H)\sigma_{xx}^2 - 2H\sigma_{xx}\sigma_{yy} + (F + H)\sigma_{yy}^2 + 2N\sigma_{xy}^2 \tag{5}$$

where the parameters F, G, H, and N can be obtained from the uniaxial plastic anisotropy coefficients R_0, R_{45} and R_{90} with the uniaxial tensile yield stress at the rolling direction σ_0.

Ferron et al. (1994) proposed a plasticity model for orthotropic sheets under a state of plane stress (σ_{xx}, σ_{yy}, σ_{xy}) along the (x, y) axes corresponding to the principal directions of in-plane anisotropy. This orthotropic yield function can be defined as:

$$f = \phi(x_1, x_2, \alpha) - \bar{\sigma}(\bar{\varepsilon}^p) \tag{6}$$

where it is assumed the assumption of isotropic work-hardening along with an equivalent stress measure defined as function of an equivalent plastic-strain, that is, $\bar{\sigma}(\bar{\varepsilon}^p)$. In Eq. (6), the variables x_1 and x_2 denote the center and radius of the Mohr's circle whereas α is the orientation angle between the in-plane principal stresses directions and the in-plane orthotropic material symmetry directions, that is, $\alpha = (x, 1) = (y, 2)$. Also, the variables x_1 and x_2 can be defined in polar coordinates as

$$x_1 = G(\theta, \alpha, \bar{\sigma}) \cos \theta \tag{7}$$

$$x_2 = G(\theta, \alpha, \bar{\sigma}) \sin \theta \tag{8}$$

The function $G(\theta, \alpha, \bar{\sigma})$ in Eqs. (7-8) represents the length of the radius to a point on the yield locus in (x_1, x_2) axes and θ is polar angle, see the yield loci plotted in Fig. 2.

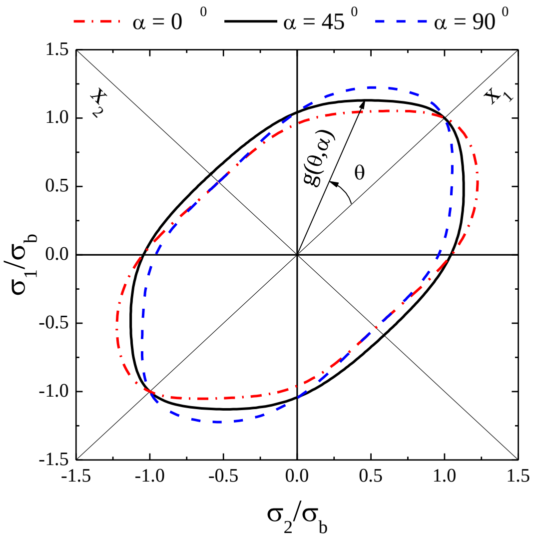

Figure 2: Schematic representation of the yield surface in principal stress space (σ_1, σ_2) normalized by the equivalent stress measure. The yield loci are parameterized by the angle α between the principal directions of orthotropy and principal stress axes. (Moreira et al., 2000).

Thanks to the isotropic expansion of the yield surface, fulfilled by the isotropic work-hardening assumption, the function $G(\theta, \alpha, \bar{\sigma})$ can be defined as:

$$G(\theta, \alpha, \bar{\sigma}) = \bar{\sigma}\, g(\theta, \alpha) \tag{9}$$

where $g(\theta, \alpha)$ represents the adimensional length of the radius to a point on the yield locus normalized by the effective stress measure $\bar{\sigma}$ which is defined as the equibiaxial yield stress. The yield loci obtained with Ferron's orthotropic plasticity criterion are plotted in Fig. 2.

For finite element implementation purposes, Ferron's yield function is defined as:

$$\phi(x_1, x_2, \alpha) = \left\{ \begin{array}{l} \left[\dfrac{(x_1^2 + A\,x_2^2)^3 - k\,x_1^2 (x_1^2 - B\,x_2^2)^2}{(1-k)} \right]^{m/6} \\ -\dfrac{2a}{(1-k)^{\mathrm{m}/6}} \dfrac{x_2\,x_1^{2n-1}}{(x_1^2 + x_2^2)^{n-m/2}} \cos 2\alpha \\ +\dfrac{\mathrm{b}}{(1-k)^{\mathrm{m}/6}} \dfrac{x_2^{2p}}{(x_1^2 + x_2^2)^{p-m/2}} \cos^{2q} 2\alpha \end{array} \right\}^{1/\mathrm{m}} \tag{10}$$

In Eq. (10), the exponents m, n, p and q are known a priori while the material parameters A, B, k, a and b can be obtained in two steps. Firstly, the parameters (A, B and k) are calculated from the stress-ratios (σ_b/σ_{45}) and (σ_b/τ_0) between the equibiaxial yield stress, σ_b, and the uniaxial yield stress at 45^0 with respect to the rolling direction, σ_{45}, and the shear yield stress, τ_0, along the rolling direction, respectively, and the plastic anisotropy coefficient, R_{45}. For steels, the usual values for the exponents are m = 2, n = 1 or 2, p = 1 or 2 and q = 1 or 2. A flattening of the yield surface near plane-strain tension/compression and pure shear stress states is obtained with k > 0. Secondly, a and b parameters describing the initial anisotropy, can be obtained from the (R_0, R_{90}) values or else from the uniaxial yield stresses (σ_0, σ_{45}, σ_{90}). Also, Hill's 48 anisotropic yield criterion can be obtained in Ferron's yield criterion by setting k = 0, m = 2 and n = p = q = 1. Ferron's orthotropic plasticity yield criterion has been implemented as user material subroutines in ABAQUS/Standard and Explicit commercial finite element codes, as detailed elsewhere (Moreira and Ferron, 2007). Both anisotropic yield criteria are adopted in the numerical simulations of the deep-drawing of a two-piece can with the factorial design to evaluate the influence of material parameters and the tribological conditions on the geometry and wall thickness strains of the stamped part. Swift's work-hardening equation, see Eq. (3), is adopted in numerical simulations. Therefore, to account for the factorial design combinations which affect the material plastic anisotropy, the parameters of Eq. (3) are defined as:

$$\sigma = K_\alpha (\varepsilon_0^\alpha + \varepsilon^p)^{N_0} \tag{11}$$

with $K_\alpha = K_0\, (\sigma_{\alpha 0})^{1+N_0}$ and $\varepsilon_0^\alpha = \varepsilon_0/\sigma_{\alpha 0}$, where $\sigma_{\alpha 0}$ is calculated by the yield criterion whereas K_0, N_0 and ε_0 are the parameters determined from the fitting of Eq. (3) at the rolling direction.

3 FINITE ELEMENT MODELLING

The deep-drawing tooling is composed of a punch, a counter-punch and two blank-holders, a lower and an upper. The tooling assembly is schematically depicted in Fig. 3. Owing to axial symmetry, only one half the view is presented. First, the blank-holders make contact with the blank. Then, both blank-holders move downwards pushing the blank against the punch. To compensate for the sheet thickening at the flange, the blank-holders move at a slightly different stroke velocity, namely, the lower blank-holder is a little bit faster. Finally, at the end of the punch stroke, the counter-punch comes down to shape the packaging bottom.

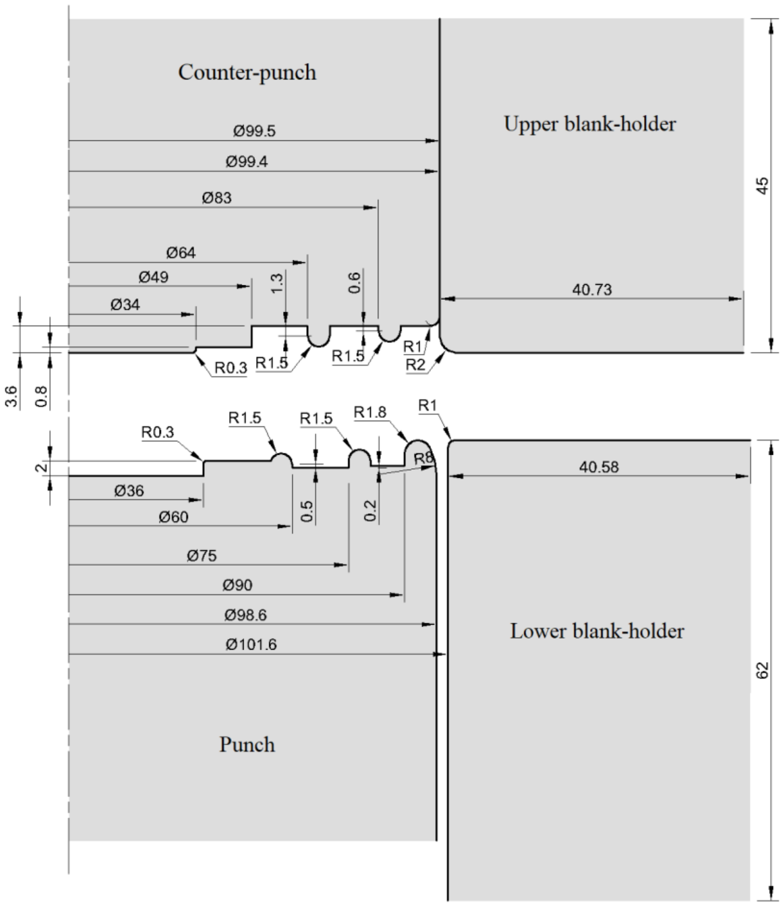

Figure 3: Deep-drawing tooling assembly. Dimensions in mm.

Owing to the axial symmetry of both tooling and blank as well as the material orthotropic symmetry, only 1/4 of the geometry was modeled. The tooling is defined by discrete rigid elements while the blank by shell elements with a mapped mesh. The mesh for the tooling used is R3D4 elements and the blank S4R elements, according to the ABAQUS terminology. Mesh refinement is adopted in the small corner radii of the tools and the corresponding zones where the blank will have contact with the tooling. The meshed tooling parts and blank are shown in Fig. 4 and the finite element mesh summary of the assembly is listed in Table 1.

Table 1. Mesh properties.

Part	Number of nodes	Number of elements	Element Type
Blank	8037	7860	S4R
Punch	5074	4920	R3D4
Counter-Punch	4870	4725	R3D3
Lower Blank-Holder	2744	2640	R3D6
Upper Blank-Holder	2544	2444	R3D5

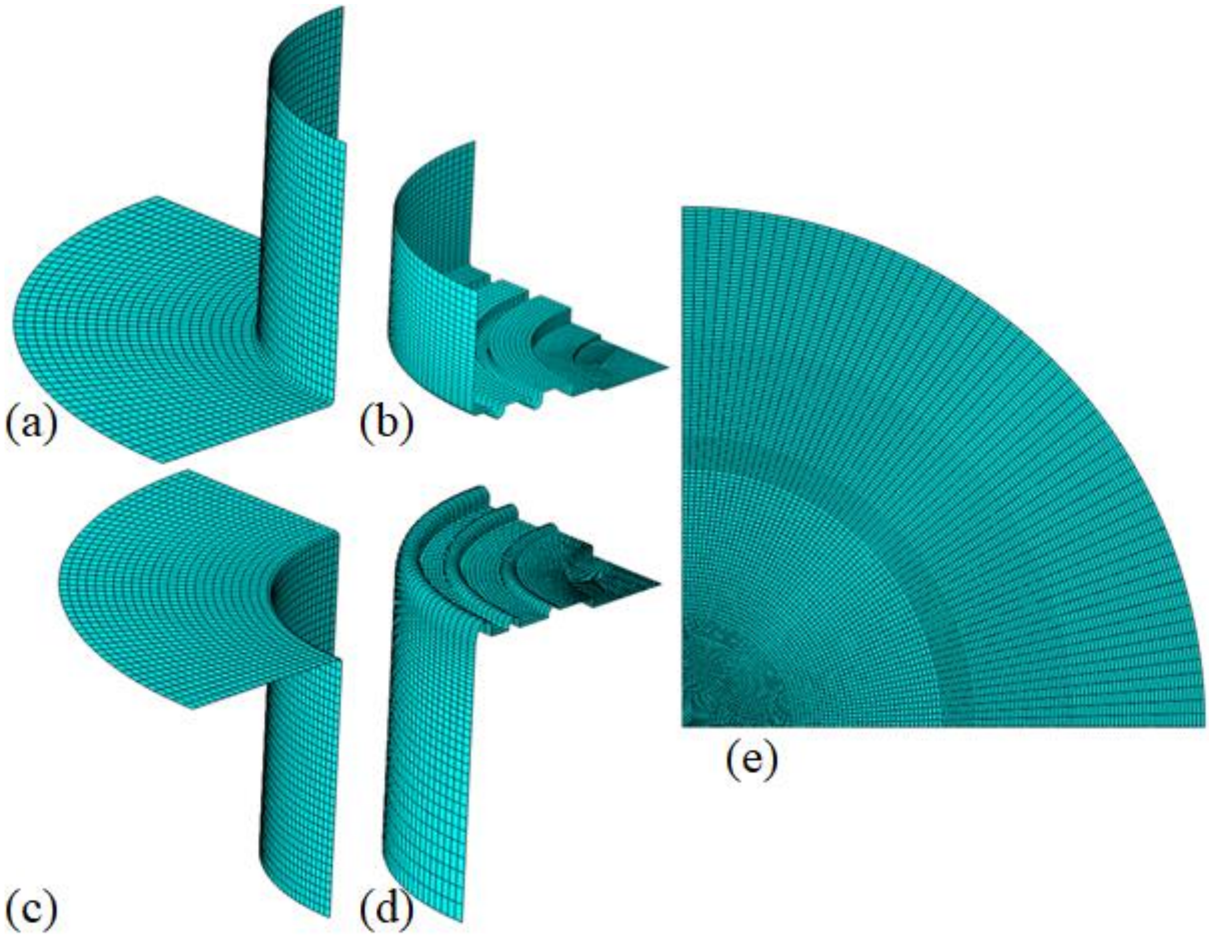

Figure 4: Finite element mesh: (a) Upper blank-holder; (b) Counter-punch; (c) Lower blank-holder; (d) Punch; (e) Blank.

The contact effects between the blank and tooling were described using Coulomb's friction law. To describe the metallic sheet's behavior, Hooke's linear isotropic elasticity was assumed, defined as a function of the Young modulus (207 GPa) and Poisson ratio (0.29), together with the hypothesis of an isotropic work-hardening of the blank in the context of plastic flow theory.

Instead of using a blank-holder force control, it is proposed to control the blank-holder displacement to avoid both excessive thinning at the punch radius and excessive grasping due to blank thickening at the flange zone. For this purpose, the lower blank-holder moves slightly faster than the upper, increasing the distance between them during the deep-drawing process. A curve to represent this distance evolution was adjusted according to the blank thickness behavior in preliminary simulations, presenting an approximated linear nature given as:

$$h_i = 0.25 + 0.25 \cdot t \tag{12}$$

in which h_i is the increasing gap distance between the blank-holders in millimeters and t is the step time in seconds.

To meet the required production rate of 100 two-piece packaging cans per minute, the deep-drawing process was simulated in an interval of 0.6 seconds. Since the process can be split in the drawing of the packaging body and the drawing of the bottom, individual steps were created for each of these stamping operations. To equalize the lower and upper blank-holders with the counter-punch speed, in the first step both the blank-holders travel 48 mm in 0.558 seconds, while the counter-punch travels 36.1 mm in 0.042 seconds. Two additional steps were created just to represent the blank-holders griping and releasing the blank at the beginning and at the end of the simulation. The simulation steps are summarized in Table 2.

Table 2. Steps of the deep-drawing simulation of two-piece can.

Step	Step time (sec.)
Gripping	0.005
Deep-Drawing	0.558
Bottom Drawing	0.042
Release	0.050
Total	0.655

4 FACTORIAL DESIGN

To evaluate how strongly each of the interest parameters influences the feasibility of packaging mass reduction using thinner blanks, a two-level 2^4 factorial design with a single replicate and a center point is proposed in this numerical study. These parameters are defined by the ratio between the Coulomb`s friction coefficients between the blank and punch (and counter-punch) and the friction coefficient between the blank and the blank-holders (μ_P/μ_{BH}); the ratio between the plastic anisotropy coefficients taken at 0 and 45 degrees with respect to the sheet rolling direction (R_0/R_{45}); the ratio between the plastic anisotropy coefficients at 90 and 45 degrees with respect to the sheet rolling direction (R_{90}/R_{45}); and the initial blank thickness (h). The values adopted in each design level and the design matrix are listed in Table 3. The center point corresponds to initial design conditions. For the plastic anisotropy coefficients ratios, R_{45} was kept constant while adjusting the values of R_0 and R_{90} coefficients. For the friction coefficient, the lower (and the upper) blank-holder friction coefficient μ_{BH} was kept constant equal to 0.05 while adjusting the punch (and the counter-punch) friction coefficient μ_P-value.

The forecasted effect of each combination of parameters can be calculated by Eq. (13), while their sum of squares ($SS_{A,B,\ldots,K}$) is given by Eq. (14):

$$A, B, \ldots, K = \frac{1}{8} Contrast_{A,B,\ldots,K} \tag{13}$$

$$SS_{A,B,\ldots,K} = \frac{1}{nr \cdot 2^k} \left(Contrast_{A,B,\ldots,K}\right)^2 \tag{14}$$

Proceedings of the XXXVIII Iberian Latin-American Congress on Computational Methods in Engineering
P.O. Faria, R.H. Lopez, L.F.F. Miguel, W.J.S. Gomes, M. Noronha (Editores), ABMEC, Florianópolis, SC, Brazil, November 5-8, 2017.

where nr denotes the number of replicates in the factorial design and k the number of factors, which in this case, is four. The $Contrast_{A,B,\ldots,K}$ is the summation of the results of every combination, following the algebraic signs in Table 4. Positive effects indicate that the result is directly proportional to that factor, while negative effects indicate an inversely proportional relationship.

Table 3. The design matrix for the proposed 2^4 factorial design.

Parameter	Label	Adopted levels			Treatment combination	A	B	C	D
		Low	Center	High					
μ_P/μ_{BH}	A	1.5	2	2.5	-1	-1	-1	-1	-1
R_0/R_{45}	B	0.4	0.7	1	a	1	-1	-1	-1
R_{90}/R_{45}	C	0.4	0.7	1	b	-1	1	-1	-1
h (mm)	D	0.175	0.194	0.213	c	-1	-1	1	-1
					d	-1	-1	-1	1
					ab	1	1	-1	-1
					ac	1	-1	1	-1
					ad	1	-1	-1	1
					bc	-1	1	1	-1
					bd	-1	1	-1	1
					cd	-1	-1	1	1
					abc	1	1	1	-1
					abd	1	1	-1	1
					acd	1	-1	1	1
					bcd	-1	1	1	1
					abcd	1	1	1	1
					Center	0	0	0	0

Since a successfully stamped two-piece can must be obtained without any defects such as wrinkling, localized necking or even fractured zones, the main result aimed here is the thickness strain variation along the wall of the two-piece can. Neglecting the flange zone and part of the cup wall wherein the wrinkles may appear under compressive orthoradial and radial straining, most of the stamped regions are submitted to negative thickness strains which can result in localized necking and final fracture. Therefore, the modulus of the thickness strain values is adopted to keep the correct interpretation of the signs resulting from the estimated effects. Next, the total sum of squares is given by:

$$SS_T = \sum_{i}^{2}\sum_{j}^{2}\sum_{k}^{2}\sum_{l}^{2}\sum_{m}^{n} y_{ijklm}^2 - \frac{y_{\ldots}^2}{nr \cdot 2^k} \tag{15}$$

The first right-hand term of the Eq. (15) provides the summation over the square of each response y, while the second right-hand term defines the corresponding mean value obtained by squaring the total sum of all 16 responses. For the variance analysis, the mean square (MS) and variance (F_0) values are:

$$MS_{A,B,\ldots,K} = \frac{SS_{A,B,\ldots,K}}{DOF_{A,B,\ldots,K}} \tag{16}$$

$$F_0 = \frac{MS_{A,B,\ldots,K}}{MS_E} \tag{17}$$

where $DOF_{A,B,\ldots,K}$ is the degree of freedom of the corresponding effect and MS_E is the mean square error. It should be noted that in a single replicate design, there is no internal error estimate. One approach to deal with it is to assume that certain high-order interactions are negligible and, thus, the error estimate can be calculated by combining the mean square values of those interactions.

Table 4. Contrast constants for the 2^4 design (Montgomery, 1997).

	A	B	AB	C	AC	BC	ABC	D	AD	BD	ABD	CD	ACD	BCD	ABCD
(1)	-	-	+	-	+	+	-	-	+	+	-	+	-	-	+
a	+	-	-	-	-	+	+	-	-	+	+	+	+	-	-
b	-	+	-	-	+	-	+	-	+	-	+	+	-	+	-
ab	+	+	+	-	-	-	-	-	-	-	-	+	+	+	+
c	-	-	+	+	-	-	+	-	+	+	-	-	+	+	-
ac	+	-	-	+	+	-	-	-	-	+	+	-	-	+	+
bc	-	+	-	+	-	+	-	-	+	-	+	-	+	-	+
abc	+	+	+	+	+	+	+	-	-	-	-	-	-	-	-
d	-	-	+	-	+	+	-	+	-	-	+	-	+	+	-
ad	+	-	-	-	-	+	+	+	+	-	-	-	-	+	+
bd	-	+	-	-	+	-	+	+	-	+	-	-	+	-	+
abd	+	+	+	-	-	-	-	+	+	+	+	-	-	-	-
cd	-	-	+	+	-	-	+	+	-	-	+	+	-	-	+
acd	+	-	-	+	+	-	-	+	+	-	-	+	+	-	-
bcd	-	+	-	+	-	+	-	+	-	+	-	+	-	+	-
abcd	+	+	+	+	+	+	+	+	+	+	+	+	+	+	+

In the model variance analysis, the ordinary R^2, defined in Eq. (18), provides the measure for the proportion of total variability described by the model. However, the problem with this statistic is that it always increases as more factors are added to the model, even if some factors are not significant. The adjusted R^2 in Eq. (19) offers a statistic adjusted for the "size" of the model, actually decreasing if nonsignificant terms are added to a model (Montgomery, 1997):

$$R^2 = \frac{SS_{Model}}{SS_T} \tag{18}$$

$$R^2_{Adj} = 1 - \frac{SS_E / DOF_E}{SS_T / DOF_T} \tag{19}$$

Proceedings of the XXXVIII Iberian Latin-American Congress on Computational Methods in Engineering
P.O. Faria, R.H. Lopez, L.F.F. Miguel, W.J.S. Gomes, M. Noronha (Editores), ABMEC, Florianópolis, SC, Brazil, November 5-8, 2017.

Provided that the two-level factorial design assumes a linearity among the factor effects, it is important to perform a curvature analysis to check whether a first-order regression model is appropriate for the case studied. The addition of center points allows a sum of squares for pure quadratic curvature, given by:

$$SS_{PQ} = \frac{n_F n_C \left(\bar{y}_F - \bar{y}_C\right)^2}{n_F + n_C} \tag{20}$$

where n_F is the number of factorial design points whereas n_C is the number of center points. If there is a curvature, the difference between the average of factors y_F and the central point average y_C is accentuated and the factorial design is named as quantitative. Conversely, in absence of a curvature, the difference between y_F and y_C is small, usually lesser than 0.1, and the factorial design is referred to qualitative. If the SS_{PQ} shows that a main effects or first-order model would not be appropriate, a second-order model would be required for the solution. An alternative for this would be the addition of axial runs, resulting in a central composite design (Medeiros et al., 2010). Here, the first-order regression model adopted is defined as:

$$\hat{y} = \beta_0 + \beta_1 x_1 + \ldots + \beta_{123} x_1 x_2 x_3 + \varepsilon \tag{21}$$

where the intercept $\beta_0+\varepsilon$ is the average of all observations and the regression coefficients $\beta_1,\ldots,\ \beta_{123}$ are equal to one-half of the corresponding factor effect estimate. This method produces least squares parameter estimates (Montgomery, 1997). Then, for the x values:

$$x_{Effect} = \frac{Effect - \left(Effect_{lower} + Effect_{higher}\right)/\,2}{\left(Effect_{higher} - Effect_{lower}\right)/\,2} \tag{22}$$

Finally, by replacing Eq. (22) in Eq. (21), one can obtain the expression for the surface response as a function of the factors investigated in the proposed factorial design.

5 RESULTS AND DISCUSSION

5.1 Mechanical properties

The uniaxial tensile tests provided the average mechanical properties according to the angular orientation with respect to the rolling direction. These results are listed in Table 5, where σ_y is the yield stress at 0.2% proof-strain, ε_u is the uniform strain, ε_t is the total strain and σ_u the ultimate tensile strength. To describe the plastic behavior, Ludwik's and Swift's work-hardening equations were adjusted to the experimental stress-strain curves. The corresponding adjusted parameters are listed in Table 6. In both tables, the values in italic denote the corresponding standard deviations obtained for each mechanical property. Swift's work-hardening equation presented a better R^2 for all uniaxial tensile angular orientations evaluated and, thus, is adopted in all numerical simulations to describe the plastic behavior of the tinplate foil.

Table 5. Uniaxial tensile mechanical properties of the tinplate foil.

	Mechanical properties							
α (deg)	σ_y (MPa)	ε_u (%)	ε_t (%)	σ_u (MPa)	N	R	ΔR	$\bar{R}$
0	272 *0.67*	23.38 *0.28*	29.76 *0.36*	368 *1.33*	0.17 *0.00*	0.99 *0.05*		
45	263 *0.16*	25.83 *0.42*	36.66 *1.22*	355 *0.17*	0.18 *0.00*	1.41 *0.00*	-0.43	1.20
90	262 *2.98*	24.25 *0.52*	32.01 *1.50*	366 *0.67*	0.18 *0.00*	0.98 *0.04*		

Table 6. Adjusted work-hardening parameters obtained from the uniaxial tensile test data.

α (deg)	Ludwik				Swift			
	K (MPa)	N	σ_0 (MPa)	R^2	K (MPa)	N	ε_0	R^2
0	464.37 *2.69*	0.5989 *0.0048*	272.18 *0.62*	0.9987 *0.0001*	657.59 *3.17*	0.2652 *0.0009*	0.0402 *0.0002*	0.9999 0.0000
45	454.62 *3.34*	0.6104 *0.0040*	262.61 *0.07*	0.9991 *0.0001*	650.58 *2.01*	0.2916 *0.0027*	0.0506 *0.0007*	0.9998 *0.0000*
90	471.02 *2.22*	0.5834 *0.0132*	261.88 *3.07*	0.9989 *0.0002*	662.91 *3.50*	0.2757 *0.0047*	0.0404 *0.0019*	0.9999 *0.0001*

5.2 Finite element predictions

The thickness strains distributions determined from the numerical simulations of the deep-drawing process are plotted in Fig. 5. These numerical predictions were obtained with the nominal mechanical properties of the tinplate steel using Swift's work-hardening parameters, see Tables (5) and (6), and the anisotropic yield criteria of Hill's (1948) and Ferron et al. (1994). Since the experimental plastic anisotropy R-values taken at 0 and 90° with respect to the rolling direction are very close, see Table (5), only the thickness strains results along the rolling and 45° angular orientations are discussed here. Firstly, one can observe the critical zones of the two-piece can wherein the localized necking may take place owing to the biaxial stretching between the can bottom center and the bending/unbending at the radii of the punch tooling, close to 60 mm as depicted in Fig. 5. The thickness strains values along the rolling direction (and at 90° orientation) are larger in comparison to the strain values at 45° angular orientation, as can be observed in Fig. 5 (a) near to the wall and flange can zones, between 90 and 110 mm. These effects are ascribed to the plastic anisotropy R-values angular evolution or else to the corresponding angular evolution of uniaxial tension/compression $\sigma(\alpha)$ under orthoradial circumferential stress state at the flange edge and pure shear state at the flange zone, namely, maxima R-values (or else minima σ-values) yield higher (or lower) radial strains at the flange (Moreira et al., 2000; Moreira and Ferron, 2007).

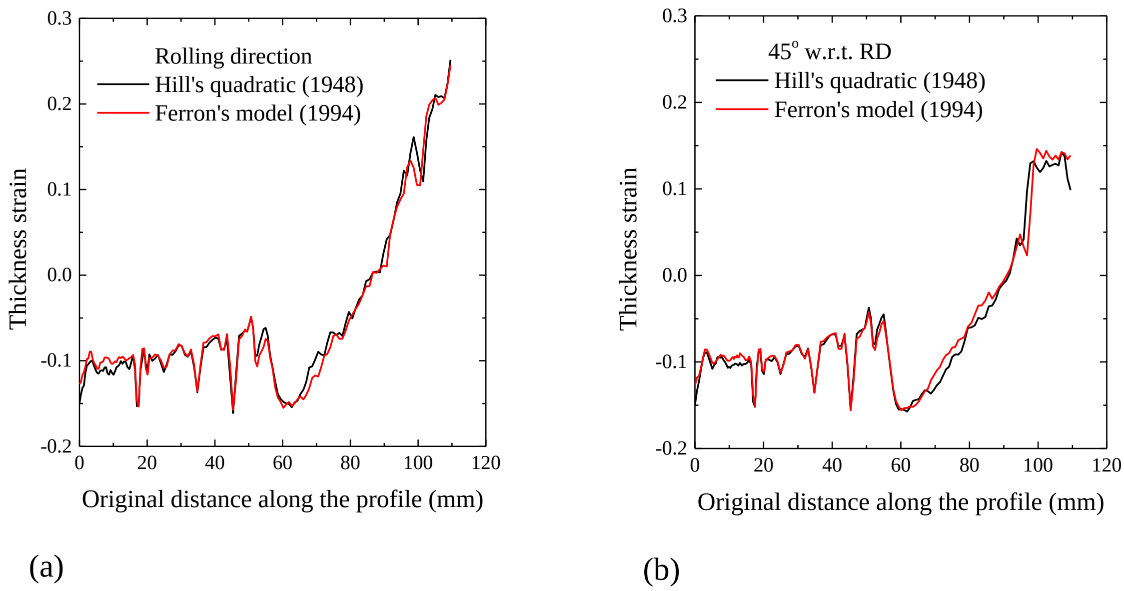

Figure 5: Numerical predictions of the thickness strains along the two-piece can profile: (a) rolling direction and (b) at 45 degrees with respect to the rolling direction.

According to the experimentally plastic anisotropy of the tinplate steel, see Table (5), observed for both anisotropy plastic-strain ratios and uniaxial tensile yield stress, specifically, $R_{45} > R_0 > R_{90}$ and $\sigma_{45} < \sigma_{90} < \sigma_0$, it is possible to analyze the earing formation at the flange of the two-piece can. The flange profile variation normalized by radial distance at the rolling direction is shown in Fig. 6. As expected, higher radial strains will produce valleys at 0^o and 90^o angular orientations with respect to the rolling direction whereas a peak or an ear is formed near to the 45^o angular orientation. It should also be noted the differences between the predictions obtained with the adopted anisotropic yield criteria, which will be addressed next.

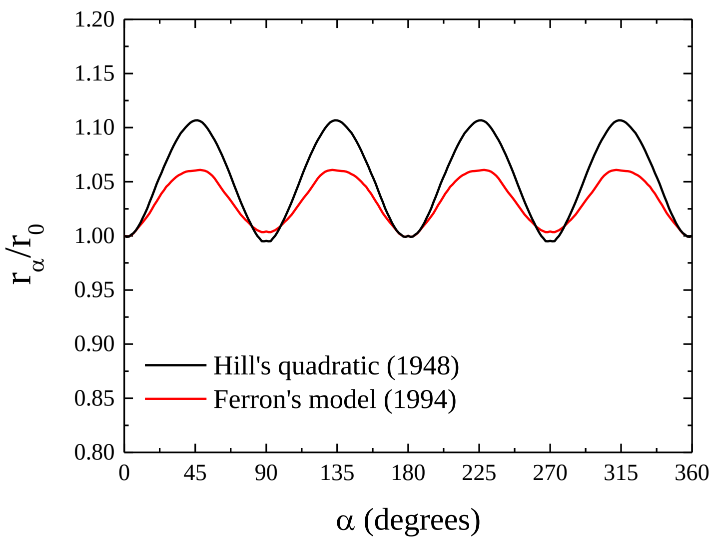

Figure 6: Predicted normalized flange profile of the tinplate two-piece can.

Proceedings of the XXXVIII Iberian Latin-American Congress on Computational Methods in Engineering
P.O. Faria, R.H. Lopez, L.F.F. Miguel, W.J.S. Gomes, M. Noronha (Editores), ABMEC, Florianópolis, SC, Brazil, November 5-8, 2017.

The forecasted ear amplitude can be explained by plotting the yield loci in the stress range of interest in the deep-drawing of circular two-piece can. This range varies from equibiaxial stretching at the can bottom, plane-strain at the can wall, pure-shear at the flange up to orthoradial compression at the flange rim. The predicted yield loci at 0° and 45° with respect to the rolling direction (RD) are plotted in Fig. 7 along with the experimental average values of the uniaxial tensile yield stress normalized by the uniaxial yield stress at RD. Hill's quadratic (1948) yield at 45° predicts lower yield stress values in whole the stress-range and, hence, provided larger radial strains (or lower thickness strains) at this angular orientation.

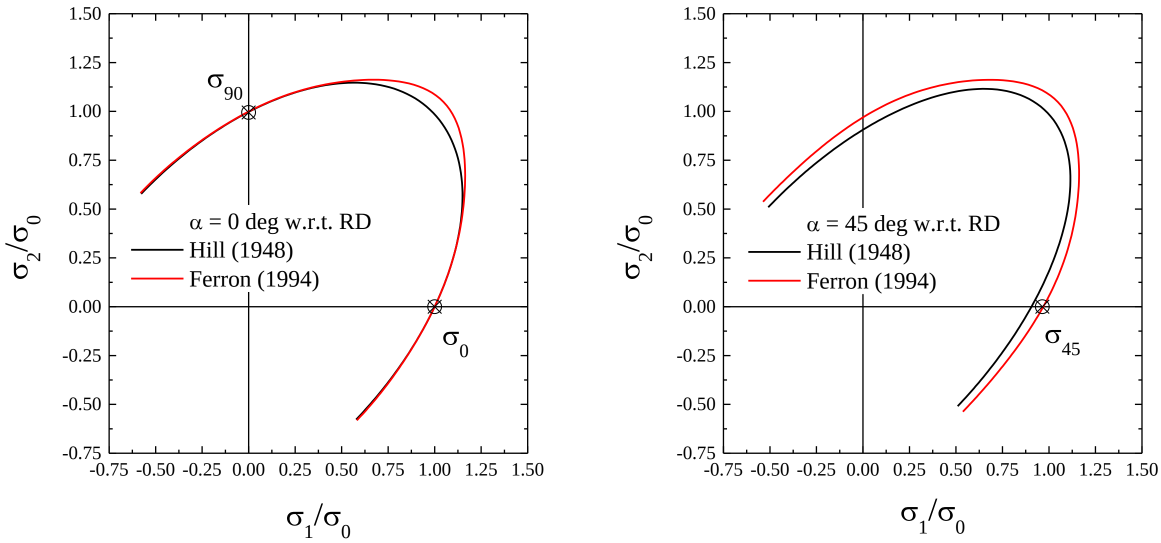

(a) (b)

Figure 7: Yield loci in the principal stress space normalized by the uniaxial tensile yield stress at rolling direction plotted at: (a) 0° and (b) 45° with respect to rolling direction.

5.3 The factorial design

For the factorial design, all the finite element simulations were performed with Hill's (1948) anisotropic yield criterion. This choice is thought to be more representative since this yield criterion can provide larger variations of the anisotropic behavior of the tinplate steel. The predictions obtained for the absolute values of wall thickness strain are listed in Table 7, as well as the estimated effects, sum of the squares and percentage of the total sum of squares. The low values obtained for the simple quadratic sum of squares suggest an absence of curvature in the present factorial design. Also, the effects of AD, ABD, ACD, BCD and ABCD combinations presented very low percental contribution and, therefore, these effects were neglected in the following analysis. The resulting variance analysis is listed in Table 8 with an adjusted R^2 of 0.9696.

From the F_0 values in Table 8, one can observe that the effect D of the initial blank thickness has a much larger impact in the factorial design. The remaining combinations with the D effect that resulted in larger thickness strains are BD and CD which, in turn, describe the influence of the plastic anisotropy coefficient at rolling and transverse directions, respectively. These combinations are expected since higher *R*-values increase the material strength resistance to thinning, which can be clearly seen in Table 7 by the negative signs in the estimated effects containing B and/or C combinations. A significant F_0 value was also obtained for the interaction BC which is the combination of the highest *R*-values together with an ideal isotropic material. Lastly, the increase of the friction coefficient between the blank and both punch tooling resulted in a low F_0 value with a positive estimated effect. Although this effect may have some influence, it will cause a weaker impact in the two-piece can wall thinning.

Table 7. Factor effect estimates and sum of squares for the 2^4 factorial design.

Combination	$\lvert\varepsilon_{thickness}\rvert$	Estimated Effects		Sum of Squares	Percent Contribution
(1)	0.156	-	-	-	-
a	0.169	A	0.006756	0.000183	2.76
b	0.166	B	-0.008250	0.000272	4.11
c	0.167	C	-0.007681	0.000236	3.56
d	0.195	D	0.031211	0.003896	58.84
ab	0.179	AB	-0.008809	0.000310	4.69
ac	0.179	AC	-0.009361	0.000351	5.29
ad	0.213	AD	0.003817	0.000058	0.88
bc	0.171	BC	-0.013209	0.000698	10.54
bd	0.194	BD	-0.005755	0.000132	2.00
cd	0.195	CD	-0.005247	0.000110	1.66
abc	0.144	ABC	-0.009570	0.000366	5.53
abd	0.214	ABD	0.000784	0.000002	0.04
acd	0.215	ACD	0.001073	0.000005	0.07
bcd	0.185	BCD	-0.000589	0.000001	0.02
abcd	0.170	ABCD	0.000298	0.000000	0.01
Center	0.159	CENTER	-	-	
SS_{PQ}				0.0005	
SS_T				0.0066	

Table 8. Variance analysis neglecting AD, ABD, ACD, BCD and ABCD.

Source of Variation	Sum of Squares	Degrees of Freedom	Mean Square	F_0
A	0.000183	1	0.000183	13.61
B	0.000272	1	0.000272	20.29
C	0.000236	1	0.000236	17.59
D	0.003896	1	0.003896	290.38
AB	0.000310	1	0.000310	23.13
AC	0.000351	1	0.000351	26.12
BC	0.000698	1	0.000698	52.01
BD	0.000132	1	0.000132	9.87
CD	0.000110	1	0.000110	8.21
ABC	0.000366	1	0.000366	27.30
Error	0.000067	5	0.000013	
Total	0.006622	15		

The first-order regression model was calculated and is presented in the form of Eq. (23). The corresponding estimated $\hat{y}$ values were subtracted from the observed y values for the calculation of the residuals. The normal probability plot of these residuals in Fig. 8 appears satisfactory.

$$\begin{aligned}\hat{y} &= 0.175796 + 0.003378x_1 - 0.004125x_2 - 0.003841x_3 + \\ &+ 0.015605x_4 - 0.004405x_1x_2 - 0.004681x_1x_3 - 0.006604x_2x_3 - \\ &- 0.002877x_2x_4 - 0.002624x_3x_4 - 0.004785x_1x_2x_3\end{aligned} \tag{23}$$

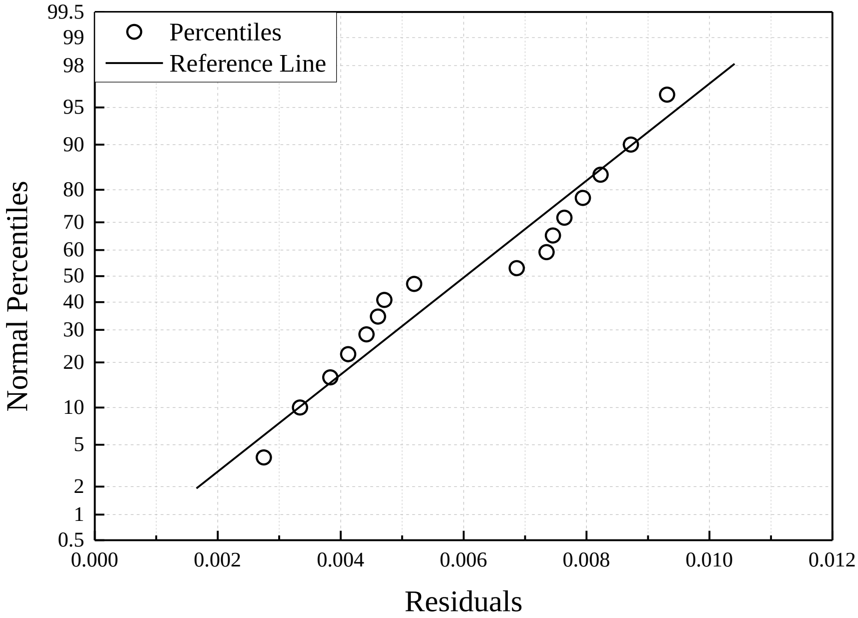

Figure 8: Normal probability plot of residuals.

By replacing the relationship between the original factors and the x variables from Eq. (22) in Eq. (21), the response surface equation is cast as:

$$\begin{aligned}\hat{y} &= -0.1261 - 0.0029A + 0.0454B + 0.0414C + 1.4969D + 0.0451AB + \\ &+ 0.0432AC + 0.1393BC - 0.5048BD - 0.4603CD - 0.1063ABC\end{aligned} \tag{24}$$

The response surface plots in Fig. 9 help illustrating the previous remarks giving more insight for the proposed factorial design analysis. Firstly, it is possible to note in Fig. 9 (a) that the first-order model provided some curvature in surface response because of BC and ABC effects in Eq. (24). Conversely, in Fig. 9 (b) it is highlighted a much stronger effect of the initial blank thickness in comparison to the friction coefficient ratio.

Proceedings of the XXXVIII Iberian Latin-American Congress on Computational Methods in Engineering
P.O. Faria, R.H. Lopez, L.F.F. Miguel, W.J.S. Gomes, M. Noronha (Editores), ABMEC, Florianópolis, SC, Brazil, November 5-8, 2017.

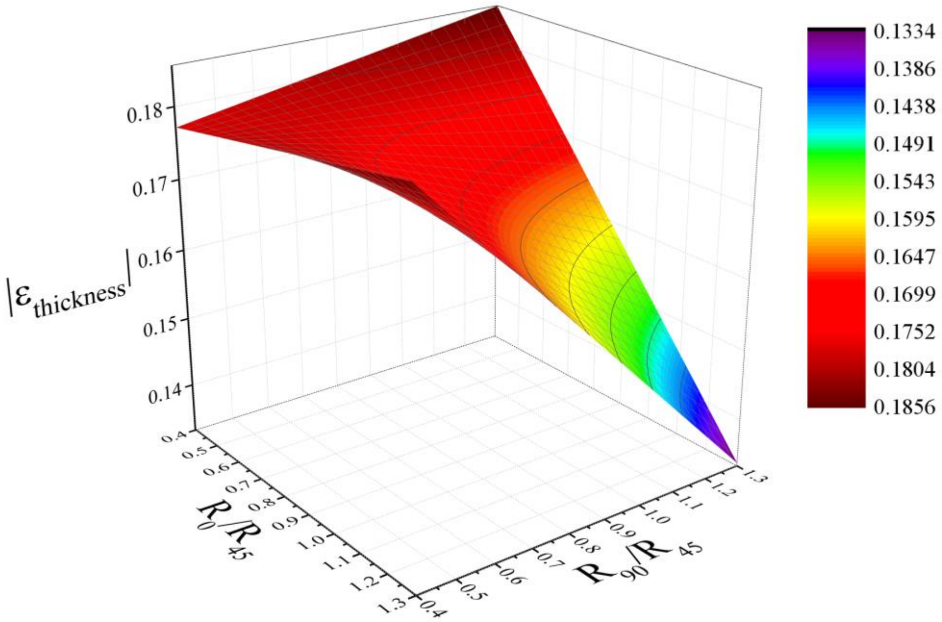

(a)

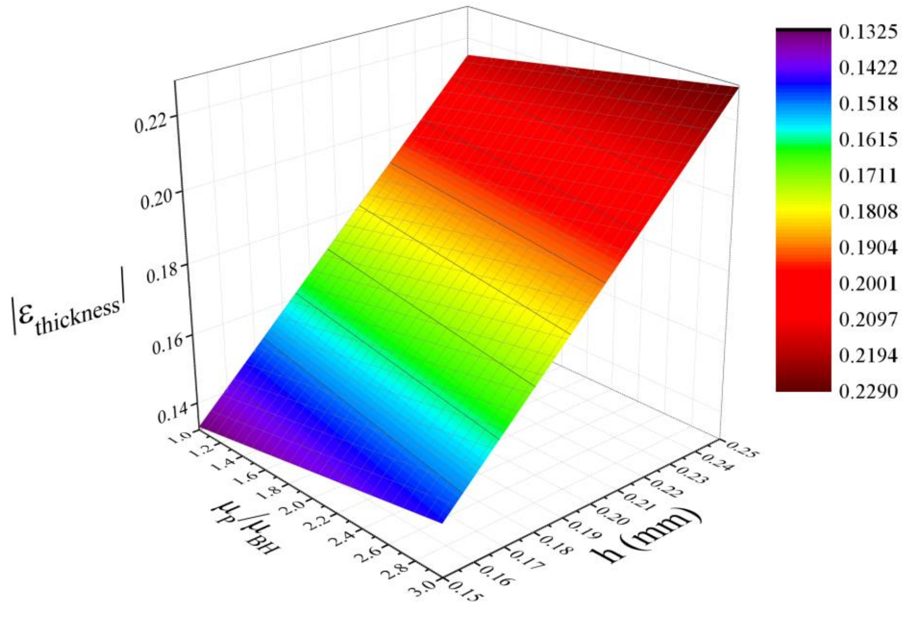

(b)

Figure 9: Response surface plots obtained for the absolute thickness strains at the wall: (a) R_0/R_{45} vs R_{90}/R_{45} with central values for μ_P/μ_{BH} and h (mm); (b) μ_P/μ_{BH} vs h (mm) with central values for R_0/R_{45} and R_{90}/R_{45} plastic anisotropy ratios.

6 CONCLUSIONS

To evaluate the feasibility of weight reduction in the manufacturing process of metallic packaging, a two-level 2^4 factorial design with a single replicate and a center point experiment is proposed in this work by considering the effects of both process (friction conditions) and blank material (initial thickness and plastic anisotropy coefficient) parameters. Based on finite element predictions of the deep-drawing of a thin tinplate sheet for forming a two-piece can, the following conclusions can be outlined:

(1) From the proposed factorial design, it is possible to classify the relevant parameters that essentially affect the wall thickness strain. The curvature investigation indicated that the affecting factors present an approximated linear interaction. Therefore, the modelling of the response surface with a first-order function is appropriate for the wall thickness strain prediction.

(2) From the performed variance analysis and the corresponding response surface generated, the parameters most affecting the wall thinning can be classified in the following order of importance: (1) initial thickness of the blank, (2) the ratio between the plastic anisotropy *R*-values measured at 0^0 and 45^o angular orientations with respect to sheet rolling direction (R_0/R_{45}), (3) the ratio between the *R*-values measured at 90^0 and 45^o angular orientations with respect to sheet rolling direction (R_{90}/R_{45}) and (4) the ratio between Coulomb friction coefficients corresponding to the blank/punch contact and the blank/blank-holders contact.

(3) To avoid the localized thinning at the bottom and punch radii regions of the two-piece can, a lower ratio between the Coulomb friction coefficients at the punch together with higher *R*-values for the tinplate material are recommended.

(4) The weight reduction of the evaluated two-piece can in this work might be envisaged as a solution of metallic packaging to face concurrent materials since a successful deep-drawn part can be achieved when the initial thickness of the blank is decreased to 0.15 mm. However, it is also highly recommended to determine the lower thickness limit value to guarantee the desired packaging strength resistance.

ACKNOWLEDGEMENTS

The authors would like to express their gratitude to CSN Research Center which supplied the tinplate material and performed the uniaxial tensile tests. The authors also acknowledge CAPES which supported this work through the graduate scholarship program (R. S. Horta and T. M. W. Ouverney) and CNPq for the PQ2 grant (L. P. Moreira).

REFERENCES

Campissi, P. R., Moreira, L. P., Alvarez, E. J. O., Viana, C. S. C., Santos, W. R., 2011. Método experimental para determinação dos limites de expansão de latas de três peças. *Tecnologia em Metalurgia, Materiais e Mineração*, vol. 8, n. 2, pp. 115–121.

Colgan, M., Monaghan, J., 2003. Deep drawing process: analysis and experiment. *Journal of Materials Processing Technology*, vol. 132, pp. 35–41.

Ferron, G., Makkouk, R. & Morreale, J., 1994. A parametric description of orthotropic plasticity in metal sheets. *Int. J. Plasticity*, vol. 10, pp. 431–449.

Hill, R., 1948. A theory of the yielding and plastic flow of anisotropic metals. *Proceedings of the Royal Academy Society of London*, vol. A193, pp. 281–297.

Marumo, Y., Saiki, H., Ruan, L., 2007. Effect of sheet thickness on deep drawing of metal foils. *Journal of Achievements in Materials and Manufacturing Engineering*, vol. 20, pp 479-482.

Medeiros, N., Moreira, L. P., Bressan, J. D., Lins, J. F. C. & Gouvêa, J. P., 2010. Upper-bound sensitivity analysis of the ECAE process. *Materials Science and Engineering A*, vol. 527, pp. 2831–2844.

Montgomery, D. C., 1997. *Design and Analysis of Experiments*. John Wiley & Sons.

Moreira, L. P., Ferron, G., 2007. Finite element implementation of an orthotropic plasticity model for sheet metal forming simulations. *Latin American Journal of Solids and Structures*, vol. 4, pp. 149–176.

Moreira, L. P., Ferron, G. & Ferran, G., 2000. Experimental and numerical analysis of the cup drawing test for orthotropic metal sheets. *Journal of Materials Processing Technology*, vol. 108, pp. 78–86

Zein, M., El Sherbiny, M., Abd-Rabou, M., El Shazly, M., 2007. Thinning and spring back prediction of sheet metal in the deep drawing process. *Materials and Design*, vol. 53, pp 797-808.